*Korean J. Chem. Eng.*, 35(3), 750-756 (2018)
DOI: 10.1007/s11814-017-0333-5

pISSN: 0256-1115
eISSN: 1975-7220

# Facile precipitation of tin oxide nanoparticles on graphene sheet by liquid phase plasma method for enhanced electrochemical properties

**Sang-Chai Kim*, Young-Kwon Park**, Byung Hoon Kim***, Hangun Kim****, Won-June Lee*****, Heon Lee*****, and Sang-Chul Jung*****,†**

*Department of Environmental Education, Mokpo National University, Muan-gun 58554, Korea
**School of Environmental Engineering, University of Seoul, Seoul 02504, Korea
***Department of Dental Materials, Chosun University, Gwangju 61452, Korea
****College of Pharmacy and Research Institute of Life and Pharmaceutical Science, Sunchon National University, Sunchon 57940, Korea
*****Department of Environmental Engineering, Sunchon National University, Sunchon 57940, Korea
(*Received 26 September 2017 • accepted 1 December 2017*)

**Abstract**−A high-performance lithium ion battery (LIB) electrode was prepared by precipitating tin oxide nanoparticles on graphene powder by the liquid phase plasma (LPP) method. The particles generated by the LPP reaction are spherical $SnO_2$ nanoparticles with a size of 5-10 nm, as confirmed by a variety of analytical devices. The quantity of $SnO_2$ nanoparticles partially aggregated on the graphene sheet surface increases as the initial concentration of the tin precursor increases. The $SnO_2$/graphene nanocomposites (SGNC) electrodes prepared by the LPP method demonstrated improved cycling stability and reversible lithium storage capacity as compared to the bare graphene electrode. The precipitated tin oxide improves the lithium storage capacity, but excess tin oxide nanoparticles rather reduced the cycling stability.

Keywords: Liquid Phase Plasma, Graphene, Tin Oxide, Lithium Storage Capacity, Cycling Stability

## INTRODUCTION

As low-carbon, green growth emerges as a global issue, the green energy industry is receiving a great deal of attention. The development of energy storage devices for electric vehicles and renewable energy is one of the biggest problems that society faces. Lithium-ion batteries (LIBs) are mainly used as the power supply for smart grids and electric vehicles [1-6]. The power density and energy density of LIBs depend heavily on the properties of the cathode and anode materials [7-10]. Graphite has been used as the anode material for energy storage devices, due to its excellent conductivity and safety [11,12]. Recently, graphene-based anode materials have received a great deal of attention. Graphene has good properties for use as an anode material, because it has excellent electronic conductivity and a large specific surface area [13,14]. However, the irreversible aggregation of graphene causes poor performance and capacity loss [15]. Therefore, in order to apply it to large-scale energy storage devices, such as electric vehicles and smart grids, a constant effort needs to be made to develop anode materials with a high-capacity and long life.

$SnO_2$ is thought to be a good replacement for graphite negative electrodes, because its theoretical capacity to store Li-ions is 782 $mAhg^{-1}$, which is higher than that of graphite: 372 $mAhg^{-1}$ [16,17]. However, a problem occurs in that the electrode becomes cracked when the volume rate of change of $SnO_2$ reaches 300% during the charge-discharge of Li-ions [18]. To solve this problem, we prepared $SnO_2$/graphene nanocomposites (hereafter SGNC) by precipitating $SnO_2$ nanoparticles on the graphene powder surface. SGNC prevents the volume expansion of self-restacking in the graphene layer and $SnO_2$, thereby improving the electrochemical performance [19-26]. We used the liquid phase plasma (LPP) method to precipitate $SnO_2$ nanoparticles on the graphene surface. Recently, research into the synthesis of a plasma within a liquid phase and the generation of nanoparticles has been gaining attention [27-29]. Also, the application of nanocomposites created by the LPP process to electrode materials has been reported [30,31]. LPP using activated chemical species generated under low pressure and radicals can rapidly synthesize nanoparticles without the need to add any reducing agents. When using the LPP method, the $SnO_2$ nanoparticles were dispersed on the graphene powder used to prepare the SGNC in a one-step process. The prepared SGNC showed a high reversible lithium storage capacity.

## EXPERIMENTAL

### 1. Materials and Chemicals

Single layer graphene (XF001) was purchased from XFNANO, while tungsten electrodes (purity 99.95%) with an outer diameter of 2 mm were purchased from T.T.M. Korea, Co. Tin chloride ($SnCl_2 \cdot 2H_2O$), which was used as a precursor for the tin particles in the LPP reaction, was purchased from Junsei chemical. Cetyltrimethylammonium bromide (CTAB, $CH_3(CH_2)_{15}N(CH_3)_3Br$, Dae-

†To whom correspondence should be addressed.
E-mail: jsc@sunchon.ac.kr
Copyright by The Korean Institute of Chemical Engineers.

jung Chemicals & metals Co.) was used to disperse the graphene powder in LPP aqueous solution and to uniformly precipitate tin oxide. We used no additionally purified reagent-grade chemicals and used ultrapure water purchased from Daejung Chemical & metals Co. as the solvent.

**2. Experimental Device**

An LPP system was used to generate tin oxide nanoparticles in solution. This LPP system was composed of a power supply, reactor and cooling unit. Detailed information on the experimental setup using a similar LPP system was provided in our previous studies [29,30]. The high frequency bipolar pulse mode power supply (NTI-500W) was manufactured by Nano technology, Inc. The operating conditions were a pulse width of 5 μs, frequency of 30 kHz, and applied voltage of 250 V. The LPP reactor was of the double tube type (OD: 40 mm, H: 80 mm) with its inner space filled with reactant solution and cooling water circulating in the outer channel. On both sides of the middle of the LPP reactor, tungsten electrodes were installed at 1.0 mm intervals and ceramic insulators were installed inside.

**3. Preparation of Composites**

Under the same process conditions, tin oxide nanoparticles were precipitated on top of the graphene powder using the LPP reaction. $SnCl_2 \cdot 2H_2O$ aqueous reactant solutions with three different concentration levels (5, 10, and 15 mM) were produced using 250 mL of ultrapure water. CTAB was added to the aqueous reactant solutions with a CTAB/$SnCl_2 \cdot 2H_2O$ molar ratio of 1/4 (1.25-3.75 mM). 100 mg of graphene powder was added to these reactant solutions and ultrasonification was done for 5 min following stirring for 1 hour, thereby preparing the final aqueous reactant solutions. The reactant solution was put into the LPP reactor and the plasma was discharged for 60 min to precipitate the tin oxide nanoparticles on the graphene powders. After the LPP reaction, the surfactant and unreacted reactants were separated from the SGNC by centrifugation (4,000 rpm) and washed with DI water five times at least. The generated SGNC was dried for 48 hours at 353 K in a vacuum oven.

**4. Electrochemical Test**

We prepared a coin-cell using SGNC synthesized by the LPP method and then evaluated its electrical properties. The slurry for the coin-cell was prepared by dissolving the active material (80%), conductive agent (acetylene black, 10%), and binder (polyvinylidene fluoride, 10%) in N-methyl pyrrolidinone solvent. This slurry was coated on copper foil and dried for 1 hour at 393 K in a convection oven. It was then roll pressed and dried again at 373 K in a vacuum oven for 1 hour. The electrochemical properties were evaluated using a Galvanostat (WBC 3000s) made by Won-A Tech. Here, 1 M $LiPF_6$ in EC/DMC (1 : 1 v/v) was used as the electrolyte and a polypropylene micro-porous film was used to measure the separation membrane at a cut-off level of 0.01-2.5 V.

**5. Structural Characterization**

The physical and chemical properties of the SGNC prepared by the LPP method were evaluated by using a variety of analytical devices. An energy-dispersive X-ray spectrum (EDX), multi-purpose X-ray diffractometer (XRD, X'pert PRO MPD, PANalytical) and X-photoelectron spectroscope (XPS, Multilab 2000 system, SSK) were used to measure the chemical properties of the SGNC. A field emission transmission electron microscope (FETEM, TECNAI-20, FEI) was used to observe the morphology of the SGNC. The dispersion pattern of the tin oxide nanoparticles on the graphene powder surface was observed with an FESEM (JSM-7100F, JEOL). The crystal structure of the tin oxide nanoparticles was analyzed using a high resolution field emission transmission electron microscope (HR-FETEM, JEM-2100F, JEOL).

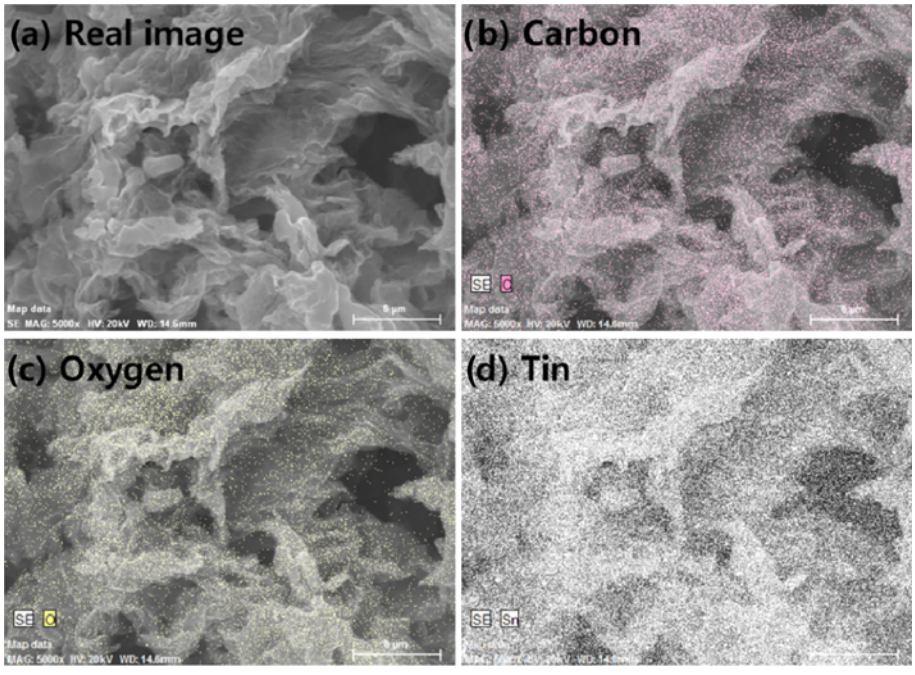


**Fig. 1. FE-SEM images of SGNC including mapped individual element of composites prepared by LPP process; (a) real SGNC image, (b) mapped tin element, and (c) mapped oxygen element.**

## RESULTS AND DISCUSSION

### 1. Characteristics of Composites

The morphology and chemical composition of the SGNC that was prepared by the LPP process were evaluated using FE-SEM. Fig. 1 shows the FE-SEM photos of the SGNC synthesized with an initial tin chloride concentration of 15 mM. Fig. 1(a) shows the real image of the SGNC that was prepared by the LPP process, and Figs. 1(b), (c) and (d) show elemental mapping for carbon, oxygen, tin contents on the surface of the graphene sheets, respectively. The graphene sheets of the SGNC are entangled with each other and scrolled, similar to crumpled paper. Meanwhile, dots that represent the carbon element of Fig. 1(b) were detected on the graphene sheets. The dots that represent the tin element of Fig. 1(d) show that it was dispersed on all of the graphene sheet surface. From this result, it can be inferred that by using the LPP process, the tin oxide nanoparticles were precipitated on the supporting material surface. Also, the dots that represent oxygen element are uniformly dispersed on the graphene sheet surface, implying that the nanoparticles which are precipitated on the surface of the graphene by the LPP reaction are composed of tin oxide. The average particle size of $SnO_2$ was determined to be 5-10 nm.

An EDX spectrum was obtained from the same SGNC sample (Fig. 1) as that used for the FE-SEM analysis shown in Fig. 2. The SGNC was prepared by the LPP reaction for 60 minutes with an initial tin chloride concentration of 15 mM. The carbon (CKa) peak at 0.28 keV in the EDX spectrum in Fig. 2 demonstrated the presence of a carbon originating from the graphene sheet. From the EDX spectra, it was determined that the composition of the nanoparticles was dominated by the tin and oxygen signals. The tin element peaks of SnKa, SnLa, SnLb, SnLb2, and SnLr were observed at 0.39 keV, 3.4 keV, 3.66 keV, 3.89 keV, and 4.13 keV, respectively, and at an energy level of 0.52 keV, an oxygen element peak of Oka was observed. This conformed with the mapping result of FE-SEM (Fig. 1(c)).

The emission peaks for Sn and O observed in the EDX spectrum show the presence of tin and oxygen elements, respectively, and confirmed the stoichiometry of the nanoparticles. Note that all SGNCs were created by the LPP reaction. The LPP process is defined as a discharge in the reactant, stabilized by the exchange of ions and electrons between the liquid and gas phases. This plasma created active chemical species in the reactant. The reactant of the desired reaction was added to the reactant solution and they reacted with the active chemical species at the interface of the liquid and gas phases. The LPP reaction was conducted in the reactant solution containing both the graphene powder and tin precursor. The tin oxide particles that were created were precipitated on the graphene sheet surface in order to synthesize the SGNC. In addition, various oxidative species (O·, $^1O_2$, $O^-_2$, $O_3$, OH·, $HO_2$, $H_2O_2$ etc.), as well as electrons, were produced at high temperature in the LPP reaction. The metal nanoparticles were oxidized into metal oxide nanoparticles by these oxidative species formed by the LPP reaction. In a previous study [29], metal oxide nanoparticles were produced during the synthesis of nanoparticles using the LPP reaction.

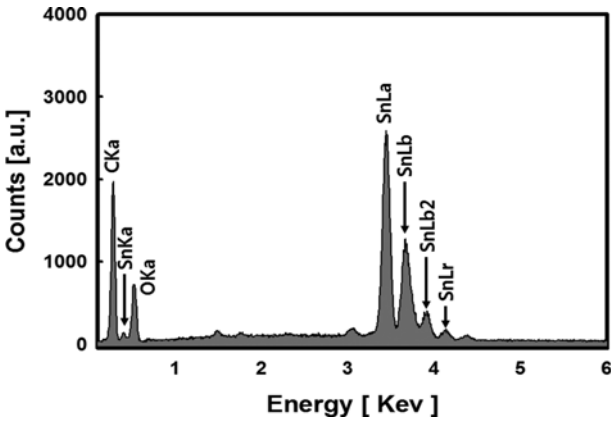


**Fig. 2. EDX spectrum of SGNC prepared by LPP process.**

**Table 1. Chemical composition of the bare graphene and SGNC synthesized by LPP reaction with different initial tin chloride concentrations**

| Samples | C | | O | | Sn | |
|---|---|---|---|---|---|---|
| | Wt% | At% | Wt% | At% | Wt% | At% |
| Bare graphene | 90.43 | 92.64 | 9.57 | 7.36 | - | - |
| 5 mM | 55.07 | 78.44 | 16.29 | 17.43 | 28.64 | 4.13 |
| 10 mM | 44.76 | 71.42 | 18.96 | 22.72 | 36.28 | 5.86 |
| 15 mM | 39.05 | 67.13 | 19.93 | 25.73 | 41.02 | 7.14 |

Table 1 shows the chemical composition of the SGNCs obtained using EDX analysis. The graphene powder used in this research was composed of 92.64 at% of carbon and 7.36 at% of oxygen. The tin content of the SGNC synthesized with initial tin chloride concentrations of 5, 10, and 15 mM was 4.13, 5.86, and 7.14 at%, respectively. As the initial precursor concentration increased, the quantity of tin element that was contained in SGNC also increased. Also, as the initial precursor concentration increased, the quantity of oxygen element within SGNC showed a tendency to increase. From these results, it can be inferred that the LPP reaction using tin chloride as a precursor was influenced by the quantity of nanoparticles that were precipitated by the precursor. Also, the precipitated nanoparticles were composed of tin oxide, which is in agreement with the result of Fig. 2.

Fig. 3 shows the image of the SGNC that was prepared using an initial precursor concentration of 15 mM. The left low magnification image of Fig. 3 shows the graphene sheet with a wrinkled morphology structure on top of the holey carbon grid. The right image with a high magnification shows that the tin oxide nanoparticles are partially aggregated on top of the layered graphene sheet. The observed tin oxide particles were approximately 5-10 nm size nanoparticles with a spherical structure.

Fig. 4 shows the HR-FETEM image of the tin oxide nanoparticles that were precipitated on the graphene sheet by the LPP reaction. The interplanar distance of 0.34 nm can be identified as corresponding to the (110) plane of the $SnO_2$ nanoparticles. The inset of Fig. 4 shows the selected area electron diffraction (SAED) pattern of the SGNC. According to the electron diffraction patterns, the two distinct diffraction rings represent (110) and (101) planes

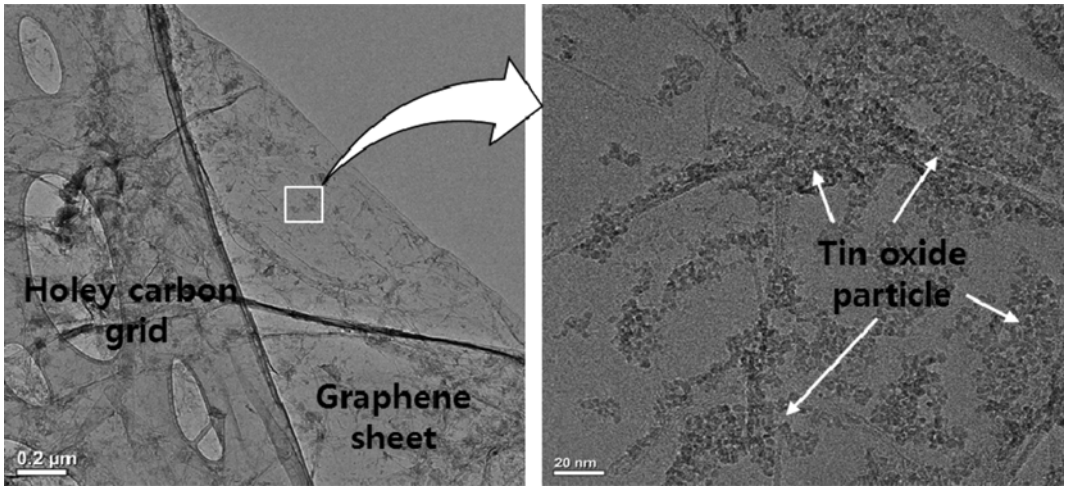


**Fig. 3. FE-TEM images of SGNC prepared by LPP method with initial tin chloride concentration of 15 mM and reaction duration of 60 min.**

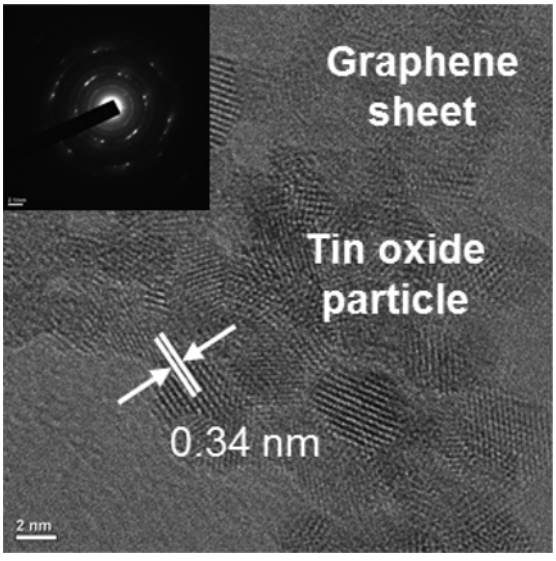


**Fig. 4. HR-FETEM image of SGNC including SAED pattern.**

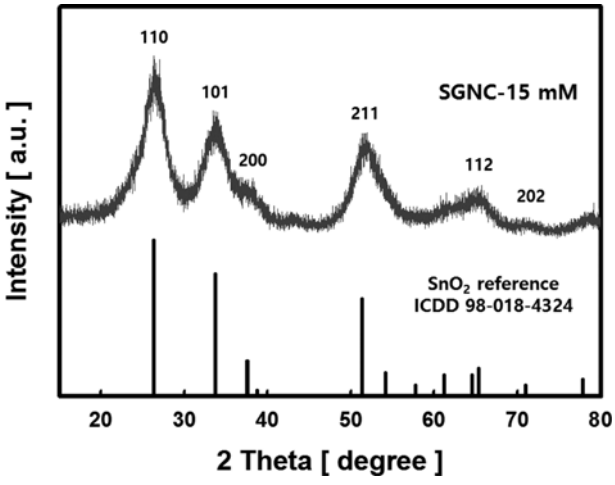


**Fig. 5. XRD patterns of SGNC prepared by LPP process with initial tin chloride concentration of 15 mM.**

from the rutile phase of the $SnO_2$ nanoparticles [32,33].

Fig. 5 shows the XRD pattern of the SGNC prepared by the LPP method with an initial precursor concentration of 15 mM. The peaks observed at 2 theta values of 26.7°, 33.9°, 51.7° and 65.3° were assigned to the (110), (101), (211) and (112) planes of rutile $SnO_2$ crystal, respectively (ICDD card no. 98-018-4324) [34,35]. The size of the D-spacing was calculated from the 2 theta values by Bragg's equation ($2d\sin\theta=n\lambda$) [35] based on the Cu anode material used in this research (K-Alpha radiation $\lambda$=1.542 Å). The crystal lattice spacings that were calculated from the observed planes were 3.39, 2.65, 1.77 and 1.43 Å, respectively. Therefore, the interplanar distance of 0.34 nm that was observed from Fig. 4 corresponds to the $SnO_2$ (110) plane of crystal face. From these results, it can be inferred that the nanoparticles that are precipitated on the surface of the graphene sheets by the LPP reaction are rutile $SnO_2$ crystals.

The surface chemistry of the SGNC obtained from the XPS

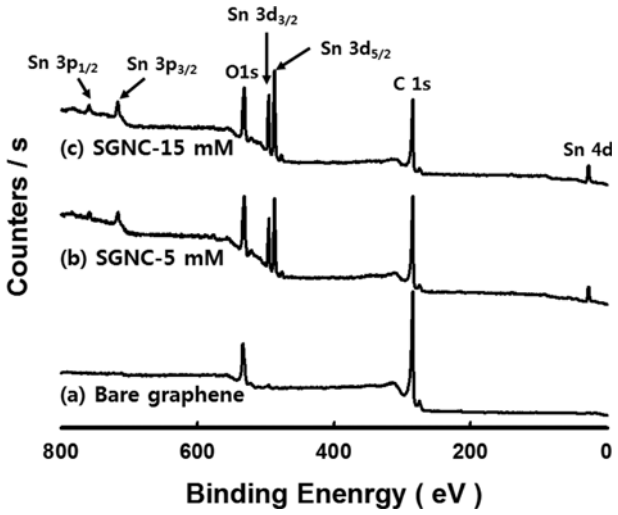


**Fig. 6. Survey XPS spectrum of bare graphene and SGNC prepared by LPP reaction with different initial precursor concentrations.**

spectra is presented in Fig. 6. Fig. 6(a) presents the general XPS spectra of the bare graphene, while shown in Figs. 6(b) and (c) those of the SGNC prepared using initial tin chloride concentrations of 5 and 15 mM, respectively. These spectra revealed the presence of tin, oxygen and carbon, while no other elements were detected [36,37]. The peak for carbon C1s that was attributed to the graphene sheets was observed at 284.6 eV, and the peak for O1s was observed at 532 eV. The observed C1s peak originated from graphite oxide and was generally assigned to the C-C bond [38]. Meanwhile, the $SnO_2$ nanoparticles generated by the LPP reaction show Sn 3d, 4d, and 3p peaks. The two peaks in the Sn 3d spectrum observed at 487.2 and 495.6 eV are attributed to the Sn $3d_{5/2}$ and Sn $3d_{3/2}$ spin orbit peaks of the $SnO_2$ nanoparticles that were precipitated on the graphene nanosheets by the LPP process, respectively [39]. As the concentration of the precursor increased, the intensity of the C1s peak decreased and the intensity of the peaks for Sn and O increased. From these results, it can be concluded that these peak intensities were influenced by the quantity of tin oxide that was generated inside the precursor within the reactant solution, which ~~is~~ in agreement with Table 1.

**2. Electrochemical Measurements**

The lithium storage performance of the SGNC electrodes prepared using different initial precursor concentrations was examined by charge-discharge cycling, and the results are shown in Fig. 7. These measurements were conducted using a WBC 3000S with a current density of 50 $mAg^{-1}$ and a cut off of voltage of 0.01-2.5 Vcm. The SGNC created by the LPP reaction showed a plateau region at the tenth cycle in the potential range of 1.2-0.8 V and, therefore, it had a slope with two regions. This was because the $SnO_2$ within the composite was reduced to Sn and, when the lithium ions were oxidized to $Li_2O$, a solid electrolyte interface (SEI) layer was formed and thus irreversible capacity loss occurred [40,41].

$$SnO_2+4Li^++4e^-\rightarrow Sn+2Li_2O \quad (1)$$

When the charge-discharge capacities at the first cycle of the bare graphene and SGNC electrodes were observed, that of the bare graphene was found to be 1,579/593 $mAhg^{-1}$ and its coulomb efficiency was 37.55%. Meanwhile, the charge-discharge capacities at the first cycle of the SGNC-5, 10 and 15 mM electrodes created by the LPP reaction were 1,662/770 $mAhg^{-1}$, 1,843/881 $mAhg^{-1}$ and 1,992/898 $mAhg^{-1}$, respectively. Also, their coulomb efficiencies were 46.32, 47.80 and 45.08%, respectively, which demonstrated that they have a higher capacity and coulomb efficiency than the bare graphene. The reason why the capacity of the SGNC electrodes was higher than that of the bare graphene electrode was because the tin oxide and Li ions, which had a high theoretical lithium storage capacity, reacted together. The electrochemical process of tin and carbon within SGNC can be represented as follows [40].

$$Sn+xLi^++xe^-\leftrightarrow Li_xSn\ (0\le x\le 4.4) \quad (2)$$

$$C+xLi^++xe^-\leftrightarrow Li_xC \quad (3)$$

The lithium storage capacities of the bare graphene and SGNC electrodes are shown in Fig. 8 as functions of the cycle number. At

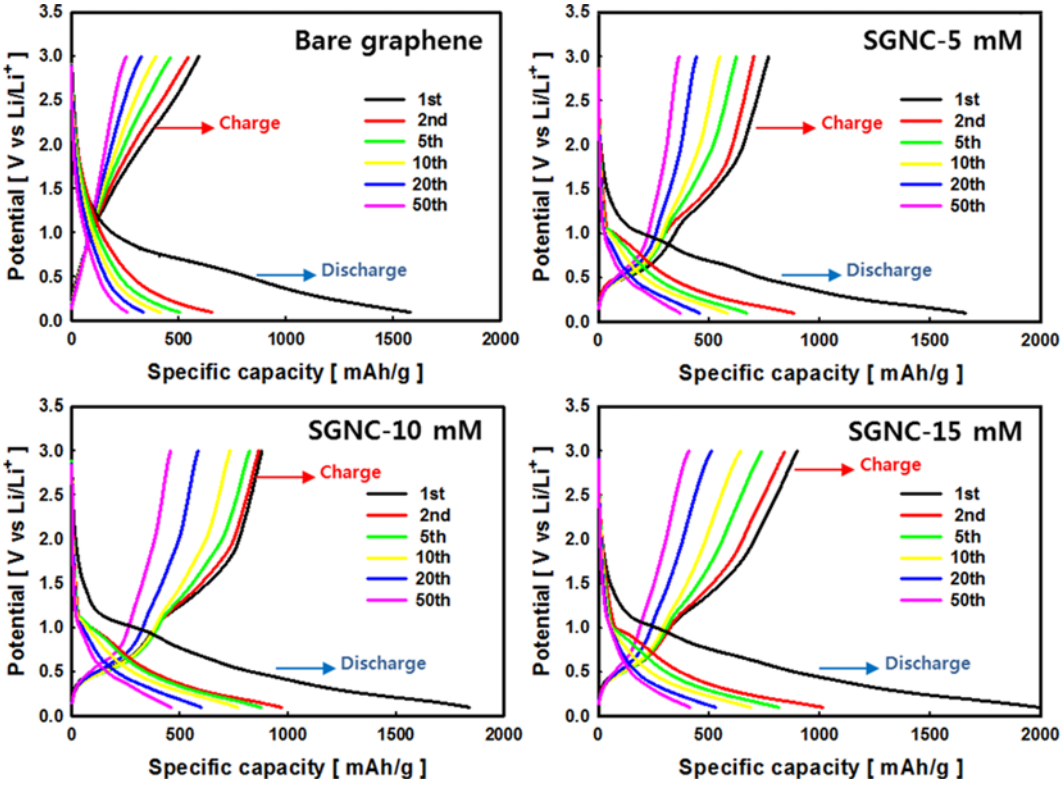


**Fig. 7. Charge-discharge curves of bare graphene and SGNC electrodes prepared under different initial precursor concentrations at a current density of 200 $mAg^{-1}$ between 3.0 and 0.01 V (vs. $Li/Li^+$).**

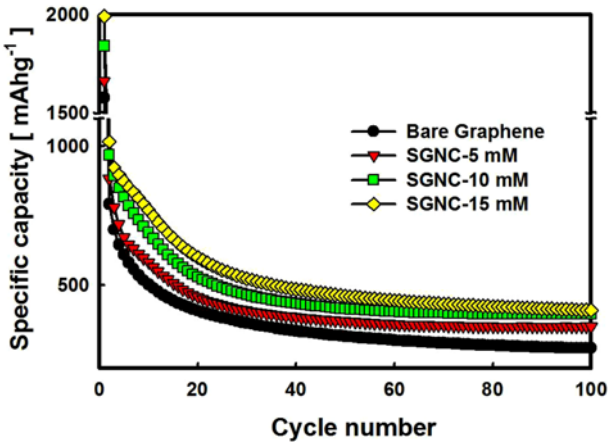


**Fig. 8. Comparison of cycling performances of bare graphene and SGNC electrodes.**

the initial stage, their capacity rapidly decreased, and after approximately 20 cycles, it slowly decreased. The capacity of the bare graphene electrode decreased from 1,579 $mAhg^{-1}$ at the first cycle to 272 $mAhg^{-1}$ at the 100th cycle, probably because of the restacking of the graphene sheets. The capacities of the SGNC-5, 10 and 15 mM electrodes were 1,662, 1,843 and 1,992 $mAhg^{-1}$, at the first cycle, and after 100 cycles they decreased to 350, 396 and 409 $mAhg^{-1}$ respectively. Especially, in the case of the SGNC-5 and 10 mM electrodes, the decline of the capacity after 100 cycles of charge-discharge was lesser, whereas the SGNC-15 mM electrode showed a continuous capacity decrease. Tin oxide has a high lithium storage capacity and expansion and aggregation occurred due to the lithium insertion/extraction reaction while undergoing the charge-discharge process. It was believed that the graphene used as a supporting material blocked the expansion and aggregation of the tin oxide's volume. Also, due to the presence of the graphene, which possesses excellent electronic conductivity, the electron transport was improved, thereby improving the specific capacity and cycling stability [37,42]. Meanwhile, the SGNC-15 mM electrode had a high discharge capacity, due to the doping with tin oxide, but over-doping with tin oxide led to a decrease in the cycling stability.

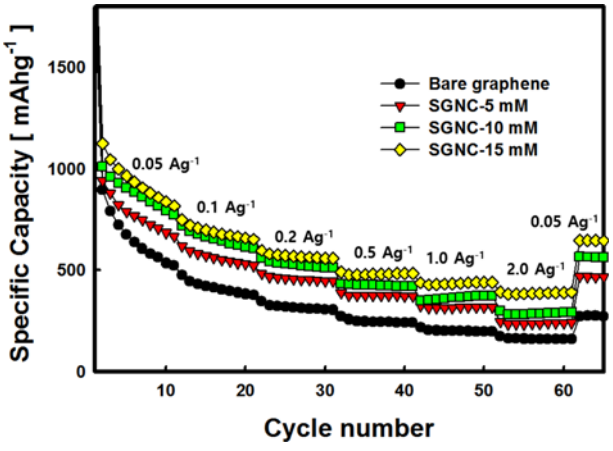


**Fig. 9. The rate discharge capability for bare graphene and SGNC electrodes.**

Fig. 9 compares the rate performance of bare graphene electrode against all other SGNC electrodes fabricated using LPP process under varying discharge current density between 0.05 and 2.0 A/g. As illustrated, it is evident that the specific capacity of all SGNCs was significantly higher than that of bare graphene, regardless of the applied current density. Specifically, the specific capacity increased with the amount of tin oxide immobilized on SGNC electrodes. We also found that SGNC electrodes better maintained the specific capacity with increasing current density (from 0.05 to 2.0 A/g) than bare graphene electrode. In fact, when current density was switched from 2 to 0.05 A/g again, bare graphene lost 45% of its initial specific capacity at the tenth cycle. In contrast, approximately 71 to 80% of specific capacity was retained for all SGNC electrodes.

## CONCLUSION

The liquid phase plasma method was used to precipitate tin oxide nanoparticles on graphene powder and to create a high-performance LIB electrode. The following results were obtained:

1. The particles generated by the LPP process are $SnO_2$ nanoparticles, as confirmed by the EDX, XRD and XPS analyses.
2. Spherical $SnO_2$ particles with sizes of 5-10 nm were fixed on the graphene sheets with partial aggregation.
3. The quantity of $SnO_2$ nanoparticles precipitated on the graphene sheets increased with increasing initial concentration of the tin precursor.
4. The SGNC electrodes prepared by the LPP method demonstrate improved cycling stability and reversible lithium storage capacity compared with the bare graphene electrode.
5. Doping the tin oxide leads to a high discharge capacity, but over-doping leads to decreased cycling stability.

## ACKNOWLEDGEMENT

This work was supported by the Technology Innovation Program (10050391, Development of carbon-based electrode materials with 2,000 $m^2/g$ grade surface area for energy storage devices) funded by the Ministry of Trade, Industry & Energy (MI, Korea).

## REFERENCES

1. M. Armand and J. M. Tarascon, *Nature*, **451**, 652 (2008).
2. D. L. Vu and J. W. Lee, *Korean J. Chem. Eng.*, **33**, 514 (2016).
3. P. G. Bruce, B. Scrosati and J. M. Tarascon, *Angew. Chem. Int. Ed.*, **47**, 2930 (2008).
4. Y. Cao, L. Xiao, W. Wang, D. Choi, Z. Nie, J. Yu, L. V. Saraf, Z. Yang and J. Liu, *Adv. Mater.*, **23**, 3155 (2011).
5. L. Ji, Z. Lin, M. Alcoutlabi and X. Zhang, *Energy Environ. Sci.*, **4**, 2682 (2011).
6. K. M. Kim, L. R. Hepowit, J. C. Kim, Y. G. Lee and J. M. Ko, *Korean J. Chem. Eng.*, **32**, 717 (2015).
7. K. S. Park, A. Benayad, D. J. Kang and S. G. Doo, *J. Am. Chem. Soc.*, **130**, 14930 (2008).
8. Z. D. Huang, X. M. Liu, S. W. Oh, B. Zhang, P. C. Ma and J. K.

Kim, *J. Mater. Chem.*, **21**, 10777 (2011).
9. L. Shen, C. Yuan, H. Luo, X. Zhang, K. Xu and Y. Xia, *J. Mater. Chem.*, **20**, 6998 (2010).
10. N. Venugopal, W. S. Kim and T. Yu, *Korean J. Chem. Eng.*, **33**, 1500 (2016).
11. J. Lin, Z. W. Peng, C. S. Xiang, G. D. Ruan, Z. Yan, D. Natelson and J. M. Tour, *ACS Nano*, **7**, 6001 (2013).
12. P. Z. Wang, B. Qiao, Y. C. Du, Y. F. Li, X. S. Zhou, Z. H. Dai and J. C. Bao, *J. Phys. Chem. C*, **119**, 21336 (2015).
13. B. Wang, H. B. Wu, L. Zhang and X. W. Lou, *Angew. Chem. Int. Ed.*, **52**, 4165 (2013).
14. H. Bai, C. Li and G. Q. Shi, *Adv. Mater.*, **23**, 1089 (2011).
15. Y. Wang, H. J. Zhang, L. Lu, L. P. Stubbs, C. C. Wong and J. Lin, *ACS Nano*, **4**, 4753 (2010).
16. Y. Chen, B. Song, R. M. Chen, L. Lu and J. Xue, *J. Mater. Chem. A*, **2**, 5688 (2014).
17. H. Park, D. H. Yeom, J. Y. Kim and J. K. Lee, *Korean J. Chem. Eng.*, **32**, 178 (2015).
18. Y. Wang, J. Y. Lee and H. C. Zeng, *Chem. Mater.*, **17**, 3899 (2005).
19. X. S. Zhou, Y. X. Yin, L. J. Wan and Y. G. Guo, *J. Mater. Chem.*, **22**, 17456 (2012).
20. W. Wei, S. B. Yang, H. X. Zhou, I. Lieberwirth, X. L. Feng and K. Mullen, *Adv. Mater.*, **25**, 2909 (2013).
21. Y. J. Gong, S. B. Yang, L. Zhan, L. L. Ma, R. Vajtai and P. M. Ajayan, *Adv. Funct. Mater.*, **24**, 125 (2014).
22. R. H. Wang, C. H. Xu, J. Sun, L. Gao and H. L. Yao, *ACS Appl. Mater. Interfaces*, **6**, 3427 (2014).
23. M. Ebner, F. Marone, M. Stampanoni and V. Wood, *Science*, **342**, 716 (2013).
24. X. S. Zhou, L. J. Wan and Y. G. Guo, *Adv. Mater.*, **25**, 2152 (2013).
25. X. S. Zhou, Z. H. Dai, S. H. Liu, J. C. Bao and Y. G. Guo, *Adv. Mater.*, **26**, 3943 (2014).
26. M. Cao, M. Zhang, L. Xing, Q. Wang and X. Y. Xue, *J. Alloys Compd.*, **694**, 30 (2017).
27. S. H. Sun and S. C. Jung, *Korean J. Chem. Eng.*, **33**, 1075 (2016).
28. D. J. Lee, S. J. Kim, J. H. Lee, H. Lee, H. K. Kim and S. C. Jung, *Sci. Adv. Mater.*, **6**, 1599 (2014).
29. S. C. Kim, B. H. Kim, S. J. Kim, Y. S. Lee, H. G. Kim, H. Lee, S. H. Park and S. C. Jung, *J. Nanosci. Nanotechnol.*, **15**, 228 (2015).
30. H. Lee, S. H. Park, S. J. Kim, Y. K. Park, B. J. Kim, K. H. An, S. J. Ki and S. C. Jung, *Int. J. Hydrogen Energy*, **40**, 754 (2015).
31. H. Lee, B. H. Kim, Y. K. Park, K. H. An, Y. J. Choi and S. C. Jung, *Int. J. Hydrogen Energy*, **41**, 7582 (2016).
32. D. Wang, X. Li, J. Wang, J. Yang, D. Geng, R. Li, M. Cai, T. K. Sham and X. Sun, *J. Phys. Chem. C*, **116**, 22149 (2012).
33. C. Zhang, X. Peng, Z. Guo, C. Cai, Z. Chen, D. Wexler, S. Li and H. Liu, *Carbon*, **50**, 1897 (2014).
34. C. Tan, J. Cao, A. M. Khattak, F. Cai, B. Jiang, G. Yang and S. Hu, *J. Power Sources*, **270**, 28 (2014).
35. S. Li, Y. Wang, C. Lai, J. Qiu, M. Ling, W. Martens, H. Zhao and S. Zhang, *J. Mater. Chem. A*, **2**, 10211 (2014).
36. L. Liu, M. An, P. Yang and J. Zhang, *Scientific Reports*, **5**, 9055 (2015).
37. L. Li, A. Kovalchuk and J. M. Tour, *Nano Res.*, **7**, 1319 (2014).
38. Y. Wang, S. Chou, H. Liu and S. Dou, *Carbon*, **57**, 202 (2013).
39. Y. Jiang, Y. Li, P. Zhou, S. Yu, W. Sun and S. Dou, *ACS Appl. Mater. Interfaces*, **7**, 26367 (2015).
40. H. Xu, L. Shi, Z. Wang, J. Liu, J. Zhu, Y. Zhao, M. Zhang and S. Yuan, *ACS Appl. Mater. Interface*, **7**, 27486 (2015).
41. Q. Guo and X. Qin, *ECS Solid State Letters*, **2**, M41 (2014).
42. X. Zhu, Y. Zhu, S. Murali, M. D. Stoller and R. S. Ruoff, *J. Power Sources*, **196**, 6473 (2011).